RSC Advances

RSC Publishing

PAPER

View Article Online
View Journal | View Issue

Screening protocol for identifying inorganic oxides with anti-oxidant and pro-oxidant activity for biomedical, environmental and food preservation applications

Cite this: *RSC Advances*, 2013, **3**, 900

Randy Mellaerts,[ad] Jan Delvaux,[a] Philippe Levêque,[b] Benjamin Wuyts,[c] Guy Van den Mooter,[c] Patrick Augustijns,[c] Bernard Gallez,[b] Ive Hermans[d] and Johan Martens*[a]

Received 12th May 2012,
Accepted 14th November 2012

DOI: 10.1039/c2ra20921g

www.rsc.org/advances

Free radicals are known to play a key role in the human body. When considering potential biomaterials, their interaction with free radicals needs to be considered at an early exploratory stage. In this contribution, we identify inorganic oxides that exhibit a free radical scavenging capacity. A convenient screening protocol was developed for identifying the anti-oxidant properties of highly dispersed inorganic materials. The method compares the degradation of an organic dye with radicals in the absence and presence of the material under investigation. The radicals are generated *via* Fenton chemistry over a heterogeneous goethite catalyst in a phosphate buffer. The procedure conveniently evaluates the anti- or pro-oxidant capacity of a large set of materials with routine laboratory equipment. Semi-quantitative EPR measurements of the radical concentration using a spin-trapping agent were used to validate the screening procedure. Besides the documented cerium oxide, four other materials were identified to exhibit comparable or even better anti-oxidant activity: aluminium titanate, antimony oxide, titanium silicalite-1 zeolite and titanium xonotlite; pro-oxidant activity was demonstrated for several zeolites.

1 Introduction

Reactive oxygen species (ROS), such as free radicals, play a crucial role in many processes related to human health, but also in waste water treatment and food preservation. In the human body, ROS are intermediate products in cellular respiration.[1] Low concentrations may be beneficial or even necessary for other processes such as intracellular signalling and defence against micro-organisms.[2] High ROS concentrations play, however, a role in the pathogenicity of inflammatory diseases such as ulcerative colitis and Crohn's disease.[3] Inflammation is also inevitable when a foreign material is implanted in the human body.[4] The duration and severity of the inflammatory response depends on the type of implant material. One of the features of inflammatory responses is an increased concentration of ROS in the extracellular space. The most prominent ROS are hydrogen peroxide (H_2O_2), superoxide ($O_2^{\cdot -}$), hydroxyl radicals ($^{\cdot}OH$) and peroxynitrite ($OONO^-$).[5] The increased concentration of these oxidative species can be attributed to the accumulation of inflammatory cells such as polymorphonuclear neutrophils and macrophages at the site of implant.[6] Prolonged inflammatory responses can have the consequence of more severe tissue reactions and subsequent failure of the implant.[7] Therefore, implants should be constructed using bio-compatible materials that could eliminate or reduce ROS caused by inflammation.

Titanium metal is a widely used implant material with superior biocompatibility.[8] The outstanding *in vivo* performance of titanium is well documented.[9–11] One of its important features is the presence of a titanium dioxide (TiO_2) layer covering the implant surface. This oxidized layer is reactive toward ROS.[12] The TiO_2 surface reacts with H_2O_2 to produce a Ti-peroxy gel,[13] which acts as a trap for $O_2^{\cdot -}$ radicals and other reactive species produced during inflammation.[14] In addition, the TiO_2 surface catalyzes the degradation of $OONO^-$.[15] Although *in vivo*, the situation is much more complex, and involves other processes such as the adsorption of plasma proteins and the activation of macrophages,[16] the ability of a surface to interact with ROS seems to be a prerequisite for achieving superior biocompatibility.

Recently, it was revealed that cerium oxide also has a strong anti-oxidant effect. Cerium oxide nanoparticles were demonstrated to be capable of defending neurons from free radical attack.[17] This protective effect was achieved by a single dose

[a]*Centre for Surface Chemistry and Catalysis, Kasteelpark Arenberg 23, Katholieke Universiteit Leuven, BE-3001 Heverlee, Belgium.*
E-mail: johan.martens@biw.kuleuven.be; Fax: +32 16 321998; Tel: +32 16 321637
[b]*Biomedical Magnetic Resonance Unit, Avenue Mounier 73/40, Université Catholique de Louvain, BE-1200 Brussels, Belgium*
[c]*Laboratory for Pharmacotechnology and Biopharmacy, O&N2, Herestraat 49-box 921, Katholieke Universiteit Leuven, BE-3000 Leuven, Belgium*
[d]*Institute for Chemical & Bio-Engineering, Wolfgang-Pauli-Strasse 10, ETH Zürich, CH-8093 Zürich, Switzerland*

and the *in vitro* effect could be maintained over a time period of two months. Heckert *et al.* reported cerium oxide nanoparticles to exhibit a potent superoxide dismutase (SOD) mimetic activity, the activity of which is correlated with the Ce^{3+}/Ce^{4+} ratio.[18] This observation suggested a catalytic mechanism, probably based on the reduction of Ce^{4+} and the generation of oxygen vacancies in the oxide lattice of the ceria. Karakoti *et al.* reviewed the work on cerium oxide.[19] It is clear that certain inorganic materials have the potential to degrade reactive oxygen and nitrogen species involved in inflammatory responses. Literature on anti-oxidant activity is limited to Ti- and Ce-based materials. In the area of heterogeneous catalysis many more materials have been identified as inhibitors of the (aut-)oxidation of organic substrates. Such inhibition has been interpreted as scavenging of radical species by the inorganic surfaces and consequently suppressing radical chain reactions. Zeolites especially have shown such tendencies.[20,21]

Anti-oxidants also play an important role in other scientific domains such as food preservation technology and polymer chemistry. Exposure of food to oxygen results in ROS and inevitably in oxidative deterioration. Anti-oxidants are used to extend the shelf life of food products. Commonly used organic anti-oxidants in food preservation include phenolic compounds and ascorbic acid.[22] The use of inorganic materials for food preservation has not been documented so far.

In other areas, such as waste water treatment by advanced oxidation processes (AOPs), the generation of ROS is highly desired. ROS are particularly useful for cleaning biologically toxic or non-degradable materials such as aromatics, pesticides, petroleum constituents, and volatile organic compounds in waste water. The contaminant materials are preferably converted to a large extent into stable inorganic compounds such as water, carbon dioxide and salts. Ozone, hydrogen peroxide, oxygen, and air are the main oxidants tested and applied to date in AOPs. These procedures may also be combined with specific catalysts, used to generate hydroxyl radicals.[23]

The aim of the present study is to develop a convenient screening protocol for the identification of the anti- or pro-oxidant ability of inorganic oxides, known from the field of heterogeneous catalysis and outside the area of the traditional biomaterials. This protocol is based on the inhibition of Fenton degradation of a dye molecule *via* anti-oxidant materials. A library of natural and synthetic zeolites, ordered mesoporous materials, clay minerals, chain silicates and bulk oxides were screened. Amongst 51 investigated materials, five showed a clear anti-oxidant effect, extending the list of potential materials beyond the currently known ceria and titania. While the majority of materials did not show any activity, some materials with pro-oxidant activity enhancing the Fenton reaction were identified as well. Such materials are potentially useful to support Fenton chemistry.

2 Materials and methods

2.1 Chemicals, stock solutions and candidate anti-oxidant materials library

A phosphate buffer was obtained by dissolving 0.696 g NaOH (BDH Laboratory Supplies), 7.908 g $NaH_2PO_4 \cdot H_2O$ (Merck) and 12.372 g NaCl in 2 L purified water (18.2 MΩ, Elga). The pH was adjusted to exactly 6.5 with 1 M NaOH. Methylene blue (MB) and reactive black 5 (RB5) were purchased from Biochemika and Sigma-Aldrich, respectively. A MB stock solution of 25 mg L^{-1} was prepared in the phosphate buffer. The dye concentration in RB5 stock solution was 250 mg L^{-1}. Both stock solutions were sonicated for 20 min to ensure complete dissolution of the dye. The investigated candidate anti-oxidant materials are the following: ultrastable zeolite Y (CBV 780 Zeolyst), zeolite Y (CBV 901, Zeolyst), ZSM-5 zeolite (CBV 28014, Zeolyst), ZSM-5, NH_4-beta, H-beta, boron-beta, H-mordenite zeolites (Südchemie); Ca-A, Na-A, K-A, K-L zeolites (Union Carbide); Na-Y zeolite (Zeocat); Na-X zeolite (Uetikon); niobium oxide, antimony oxide, magnesium oxide, aluminium titanate, aluminium oxide, manganese(II)oxide, manganese(III)oxide, zinc oxide, cerim oxide, molybdenum oxide, titanium oxide (anatase) (Sigma-Aldrich). The Ba-Y, Ca-X, Ba-L, Sr-L, Ca-L and Na-L were obtained by cation exchange. The origin of the natural zeolites and clay minerals was as follows: Clinoptilolite (Hungary); Erionite (Nevada); Charazite (Arizona); Mordenite (Nevada); Kaolinite (Georgia); Attapulgite (Spain); Hectorite (California); Magadiite (Kenya); Sepiolite (Tolsa, Spain); Laponite (Laporte Industries). They were ground into a fine powder before use. The zeolites Co,Ca-Y,[24] titanium silicalite-1,[25] SAPO-37,[26] SAPO-34,[27] SAPO-42,[27] AlPO-5,[27] AlPO-8,[27] SBA-15[28] were synthesized according to the indicated references. Titanium containing xonotlite was a synthetic product kindly provided by Redco Company, Belgium (SEM picture is displayed in Fig. 1).

2.2 Anti-oxidant–pro-oxidant screening protocol

5 to 30 mg goethite (FeO(OH), Sigma-Aldrich) was weighed in a 12 mL test tube. 5 mL MB or RB5 stock solution was added to

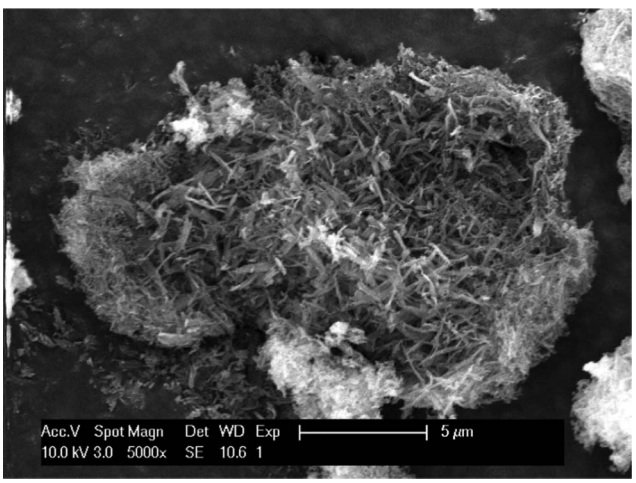

Fig. 1 SEM picture of commercially available titanium xonotlite

the test tube. The heterogeneous Fenton degradation was initiated upon addition of H_2O_2 (Fischer Scientific) at a concentration of 125, 250, 500 or 1000 mM. The reaction vessel was sealed and placed in a rotary shaker (Labinco). The reaction mixture was sampled (100 μL) after 1, 2, 4, 6, 8, 24 and 48 h and the dye concentration determined using UV-vis spectrometry in a Tecan Infinite M200 microplate reader (Tecan Benelux) in flat-bottomed, transparent 96-well plates (UV-star, Greiner Bio-One). The wavelength used for quantification was 664 nm for MB and 600 nm for RB5. Sample concentrations were calculated by linear interpolation on the calibration curve. The calibration curves were linear over a concentration range between 1 and 25 mg L^{-1} for MB and 10 and 250 mg L^{-1} for RB5. H_2O_2 quantification was performed in a similar way. A stock solution of 250 mM H_2O_2 was prepared in phosphate buffer. This was diluted (1 : 2) five times to obtain a standard series. The wavelength used for quantification was 250 nm. Sample concentrations were calculated by interpolation from the calibration curve response using a linear regression model. The calibration curve was linear over a concentration range between 10 and 250 mM.

Mannitol and phenol are organic benchmark anti-oxidants and were used as a control for the screening protocol. 125 mM organic benchmark anti-oxidant was added to the reaction. The influence of inorganic materials on the degradation of MB or RB5 was investigated by adding 10 mg to the reaction mixture. The elimination of MB or RB5 *via* adsorption on the tested oxide material – instead of oxidative degradation – was evaluated in experiments in the absence of goethite.

2.3 Nitrogen adsorption

Nitrogen adsorption isotherms at −196 °C were recorded on a Micromeritics Tristar 3000 instrument. Samples were pre-treated at 150 °C for 12 h under nitrogen flow, prior to analysis. The specific surface area was estimated using the BET model in the relative pressure range 0.05–0.2. The pore volume of porous materials was estimated using the *t*-plot method.

2.4 Scanning electron microscopy

Scanning electron microscopy (SEM) was performed on a Philips SEM XL30 FEG instrument. The samples were gold-plated prior to imaging. Displayed images are representative for the whole sample.

2.5 Spin trapping and electron paramagnetic resonance (EPR)

Phosphate buffer (2 mL) containing 8 mg goethite, 250 mM H_2O_2 and inorganic oxide (4 mg) was mixed with a magnetic stirrer for either 30 min. or 4 h. After this incubation period, the 5,5-dimethyl-pyrroline *N*-oxide (DMPO, Enzo Life Science) spin-trap was added at a concentration of 50 mM. The reaction was performed for 15 min. in the presence of DMPO. The solids were removed through filtration (Whatman SPARTAN, 0.2 μm) and a 50 μL liquid sample was collected in a capillary (Blaubrand intraMARK micropipette). The EPR spectra were acquired at room temperature using an EPR Miniscope MS-400 (Magnettech) equipped with an FC-400 resonator operating at ~9.5 GHz. The maximum microwave power level was 40 mW. Other parameters were as follows: center field 3370 G, sweep time 60 s, 1 scan per sample. The double integral of the spectra was calculated using MATLAB software version 2009b.

3 Results and discussion

3.1 Development of an anti-oxidant, pro-oxidant screening protocol

The new screening protocol for evaluating the oxidant activity of candidate materials is based on the heterogeneously catalysed oxidative Fenton degradation of a dye molecule at quasi-neutral pH. The anti-oxidant activity of a material is estimated from the inhibition of this dye degradation process. Quasi-neutral pH conditions using a phosphate buffer were selected for its relevance to the biomedical field. Goethite was selected as a heterogeneous Fenton catalyst for its proven efficiency in the catalytic decomposition of H_2O_2 into hydroxyl ($^{\cdot}OH$) and perhydroxyl ($^{\cdot}OOH$) radicals. The reasons for choosing a heterogeneous degradation with a solid-state catalyst were two-fold. A typical homogeneous Fenton reaction catalysed by dissolved iron ions (Fe^{2+}, Fe^{3+})[29] could be inhibited by the adsorption of iron ions onto the inorganic oxide under investigation. In addition, a homogeneously catalysed reaction is inhibited at quasi-neutral pH, due to the formation of insoluble Fe^{3+} hydroxide precipitates which leads to reproducibility problems. Two dye molecules were evaluated as indicator molecules: methylene blue (MB) and reactive black 5 (RB5). Fig. 2 presents the structural formula of

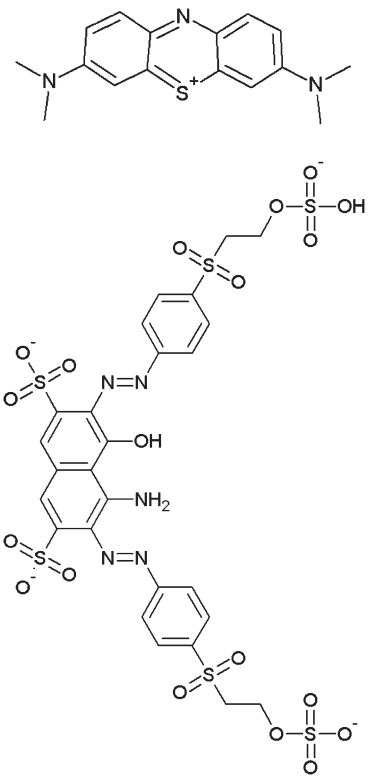

Fig. 2 Molecular formula of methylene blue (top) and reactive black 5 (bottom).

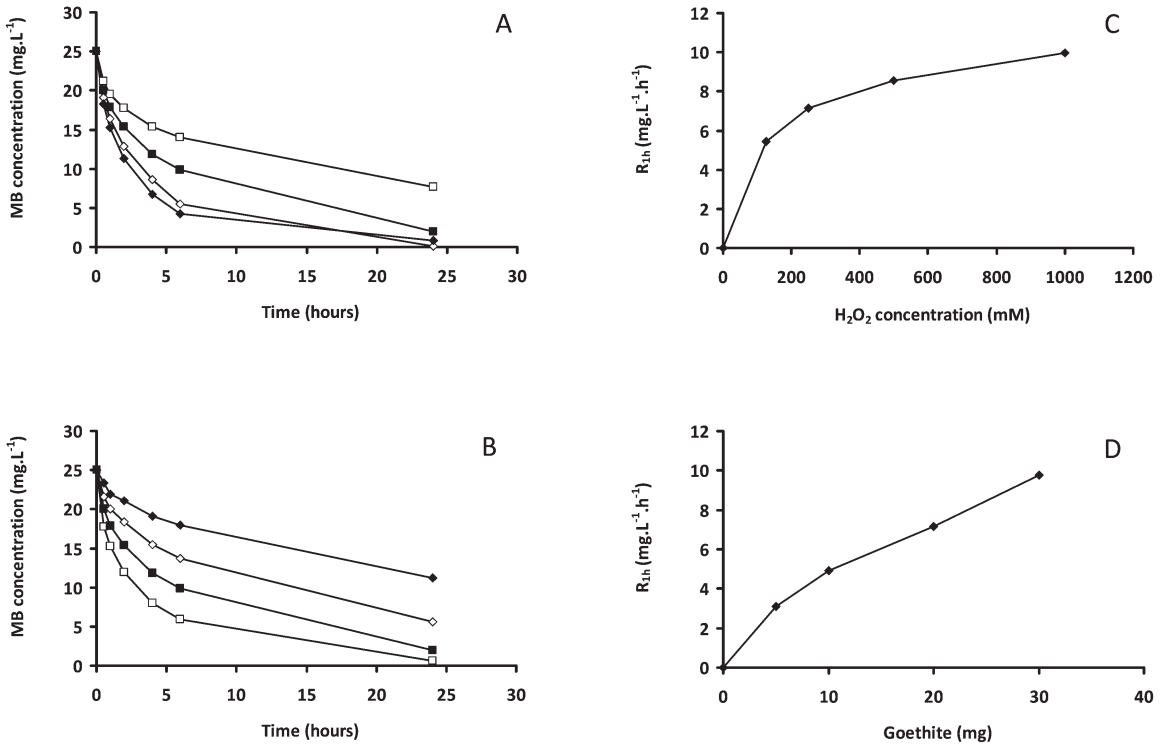

Fig. 3 Influence of the H_2O_2 and goethite concentration on the Fenton degradation of methylene blue. Experiments were performed in 5 mL phosphate buffer with (A) 20 mg goethite and varying H_2O_2 concentration: 125 mM (□), 250 mM (■), 500 mM (◇), 1000 mM (◆); (B) H_2O_2 concentration of 250 mM and varying amounts of goethite: 5 mg (◆), 10 mg (◇), 20 mg (■), 30 mg (□). The corresponding reaction rates (R_{1h}) were calculated and presented as a function of (C) H_2O_2 concentration and (D) goethite amount present in the reaction vessel.

both molecules. MB is a basic dye, extensively used for the colouring and printing of textiles. It is also popular as a medicinal dye because of its antiseptic properties. The molecular dimensions of MB are roughly estimated at 15 × 6 × 2 Å^3. MB is positively charged under quasineutral pH conditions. RB5 is a much larger dye molecule with estimated dimensions of 24 × 17 × 4 Å^3. Deprotonation of sulfonic acid groups present in the RB5 structure is responsible for its negative charge under quasi-neutral pH conditions. In the screening it is important to minimize the adsorption of the dye molecules on the investigated oxide. The selected dyes, with substantial differences in molecular dimensions and charge, enabled us to screen a wide variety of oxide materials.

In the first step, the reaction conditions for the Fenton degradation of MB were optimized. The reagent concentrations were chosen in such a way that MB degradation was sufficiently fast, while the side-reaction, generating gaseous O_2, was minimized to avoid pressure build-up in the test tube.

The time-dependent concentration of MB in the presence of different concentrations of H_2O_2 and goethite is displayed in Fig. 3. The initial reaction rate (R_{1h}) is plotted against the initial H_2O_2 concentration in Fig. 3C. At a high H_2O_2 concentration, scavenging of $^{\cdot}OH$ radicals by H_2O_2 forms the less reactive $^{\cdot}OOH$ radicals, causing the observed levelling-off in activity. The H_2O_2 concentrations of 500 mM and 1000 mM were abandoned for further research because pressure build-up in the test tubes due to the formation of gaseous O_2 was observed. Therefore, we selected 250 mM H_2O_2 for further experiments. The amount of goethite catalyst was varied from 5 mg to 30 mg. Fig. 3D shows that the MB degradation is approx. first order in goethite, as expected. Addition of 20 mg goethite was selected for further experiments. This amount was sufficient to achieve MB degradation within a convenient time of 24 h. Control experiments were performed to verify that the disappearance of MB was due to radical degradation. It was confirmed that the MB concentration remained unaltered upon addition of H_2O_2 without goethite, and in the presence of goethite without H_2O_2 (Fig. 4). This observation also implied that the adsorption of MB on goethite is negligible.

The degradation of RB5 according to the devised protocol using goethite and H_2O_2 was evaluated (Fig. 4). The RB5 concentration remained stable upon the addition of H_2O_2 without goethite, or goethite without H_2O_2, confirming the RB5 dye as an appropriate choice. The detection limit of RB5 was much higher than for MB. Therefore, it was necessary to increase the initial concentration to 250 mg L^{-1}. The degradation of this relatively high initial RB5 concentration was still incomplete after 48 h: the RB5 concentration dropped to *ca.* 200 mg L^{-1} after 8 h and *ca.* 150 mg L^{-1} after 24 h, respectively. At 48 h the RB5 concentration was *ca.* 130 mg L^{-1}. The observation that not all RB5 was degraded could be exploited in the screening of materials for oxidation activity.

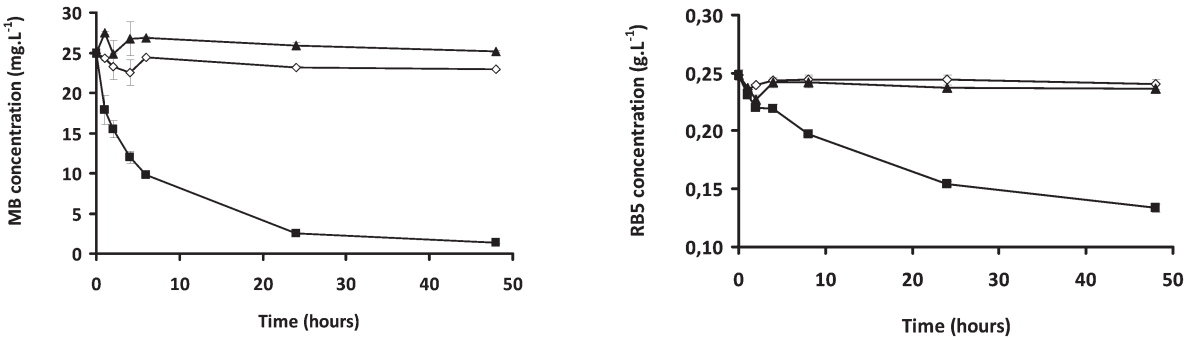

Fig. 4 Concentration of MB (left) and RB5 (right) as a function of time in presence of goethite (◇); H_2O_2 (▲); goethite and H_2O_2 (■). Experiments were performed in 5 mL phosphate buffer with 20 mg goethite and a H_2O_2 concentration equal to 250 mM.

When a pro-oxidant is added to the reaction medium, the RB5 degradation is accelerated.

Control experiments were performed using the organic benchmark anti-oxidant mannitol. Fig. 5 presents the heterogeneous degradation of MB and RB5 with the addition of 125 mM mannitol. Mannitol inhibits the degradation of both dyes. In the case of RB5, the anti-oxidant activity of phenol was also probed. Phenol is capable of inhibiting the RB5 degradation almost completely. These results support the idea that this screening protocol is well suited to identify potential anti-oxidants.

3.2 Screening of inorganic oxides for their oxidant activity

The outlined screening protocol allowed us to evaluate the anti-oxidant and pro-oxidant activity of inorganic oxides. Until now, scientific literature covering the anti-oxidant properties of inorganic materials has been limited to cerium oxide and doped analogues. This is rather surprising in view of the vast literature on heterogeneous oxidation chemistry, reporting on radical-chain inhibition and quenching effects.[20,21] We decided to screen a whole library of 51 inorganic oxides. The materials were divided into 6 material classes: (1) synthetic aluminosilicate zeolites; (2) aluminophosphate zeolites (AlPOs) and silicoaluminophosphate zeolites (SAPOs); (3) natural zeolites and clay minerals; (4) dense oxides; (5) ordered mesoporous silica materials; (6) other types. All materials and the outcome of the screening are tabulated in Table 1. For the materials that showed a positive outcome, it needs to be verified whether the material under investigation did not adsorb dye from the reaction medium, which would lead to a false positive result. Therefore, each material was investigated on its ability to adsorb MB in absence of oxidant. The outcome of this adsorption test is marked in Table 1 with "+" when the material adsorbed less than 10% of the dye molecules present in solution, and with "−" when more than 10% dye was adsorbed. When MB adsorption occurred, we performed the adsorption test with RB5, which we used at a higher concentration in the anti-oxidant capacity screening. Materials that significantly adsorb MB as well as RB5 are not suitable for the anti-oxidant capacity testing.

3.3 Inorganic oxides with an anti-oxidant capacity

The discovery of new anti-oxidant classes is of potential importance for a wide range of applications. Obvious uses of anti-oxidants are *e.g.* in food preservation, stabilization of fuels and lubricants and to prevent the oxidative degradation of polymers. Using our screening protocol, five materials were identified as anti-oxidants: (1) aluminium titanate; (2) antimony oxide; (3) cerium oxide; (4) titanium silicalite-1 and (5) titanium xonotlite (Table 1). Fig. 6 presents the RB5 concentration as a function of time for these inorganic oxides with an anti-oxidant capacity. The anti-oxidant capacity is

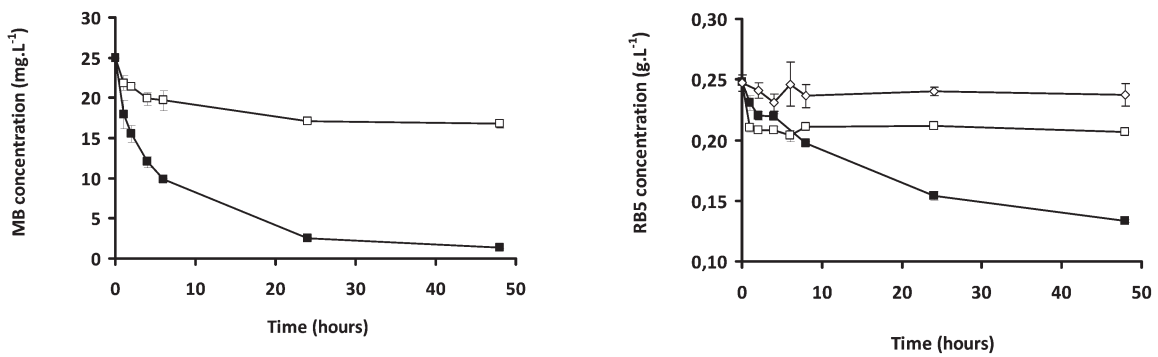

Fig. 5 Concentration of MB and RB5 as a function of time in the presence of goethite and H_2O_2 (■); goethite, H_2O_2 and mannitol (□); goethite, H_2O_2 and phenol (◇). Experiments were performed in 5 mL phosphate buffer with 20 mg goethite, 250 mM H_2O_2 and 125 mM mannitol or phenol.

Table 1 Screening the anti-oxidant and pro-oxidant capacity of inorganic oxides

Material	Adsorption test[a] MB	Adsorption test[a] RB5	Outcome
Synthetic zeolites			
CBV 780	−	+	n.e.[b]
CBV 901	−	+	n.e.
CBV 28 014	−	+	pro-oxidant
ZSM-5	−	+	n.e.
NH_4-beta	−	+	pro-oxidant
H-beta	−	+	pro-oxidant
Boron-beta	−	+	n.e.
H-mordeniet	−	+	n.e.
Na-Y	+		n.e.
H-Y	+		n.e.
Na-X	+		n.e.
Ba-Y	+		n.e.
Ca-A	+		n.e.
Na-A	+		n.e.
K-A	+		n.e.
Ca-X	+		n.e.
Ca-Z	+		n.e.
Ba-L	+		n.e.
Sr-L	+		n.e.
Ca-L	+		n.e.
Na-L	+		n.e.
CoCa-Y	−	−	
Titanium silicalite-1		+	anti-oxidant
Aluminophosphates and silicoaluminophosphates			
SAPO-37	+		n.e.
SAPO-34	+		n.e.
SAPO-42	+		n.e.
AlPO-5	+		n.e.
AlPO-8	+		n.e.
Natural zeolites and clay minerals			
Clinoptilolite	−	+	n.e.
Erionite	−	+	n.e.
Chabazite	−	+	n.e.
Mordenite	−	+	n.e.
Kaolinite	−	+	n.e.
Attpulgite	−	+	n.e.
Hectorite	−	+	n.e.
Magadite	−	+	n.e.
Sepiolite	−	+	n.e.
Laponite	−	+	n.e.
Non-porous oxides			
Niobium oxide	+		n.e.
Antimony oxide	+		anti-oxidant
Magnesium oxide	+		n.e.
Aluminium titanate	−	+	anti-oxidant
Aluminium oxide	+		n.e.
Manganese (II) oxide	+		n.e.
Manganese (III) oxide	+		n.e.
Zinc oxide	+		n.e.
Cerium oxide	+		anti-oxidant
Molybdenum oxide	+		n.e.
Titanium oxide (anatase)	+		n.e.
Ordered mesoporous silica			
SBA-15	−	−	
Other			
Titanium xonotlite		+	anti-oxidant

[a] Adsorption test "+": the material adsorbs less than 10% of the dye; "−": adsorption of the dye was more than 10%. [b] No effect.

obvious from a comparison of the RB5 dye degradation curve in the presence and absence of the material.

The strongest anti-oxidant activity was obtained with aluminium titanate and antimony oxide. Both oxides are nanomaterials with particle sizes below 100 nm and BET surface areas of 193 $m^2\ g^{-1}$ and 83 $m^2\ g^{-1}$, respectively. Aluminium titanate has previously been identified as an important high-temperature ceramic in view of its low thermal expansion coefficient, low thermal conduction, excellent thermal shock resistance, and high melting point.[30] Antimony oxide is known as a flame retardant system when used in combination with a halogen such as bromine. It acts as a catalyst, facilitating the breakdown of halogenated flame retardants to active radicals. It also reacts with the halogens to

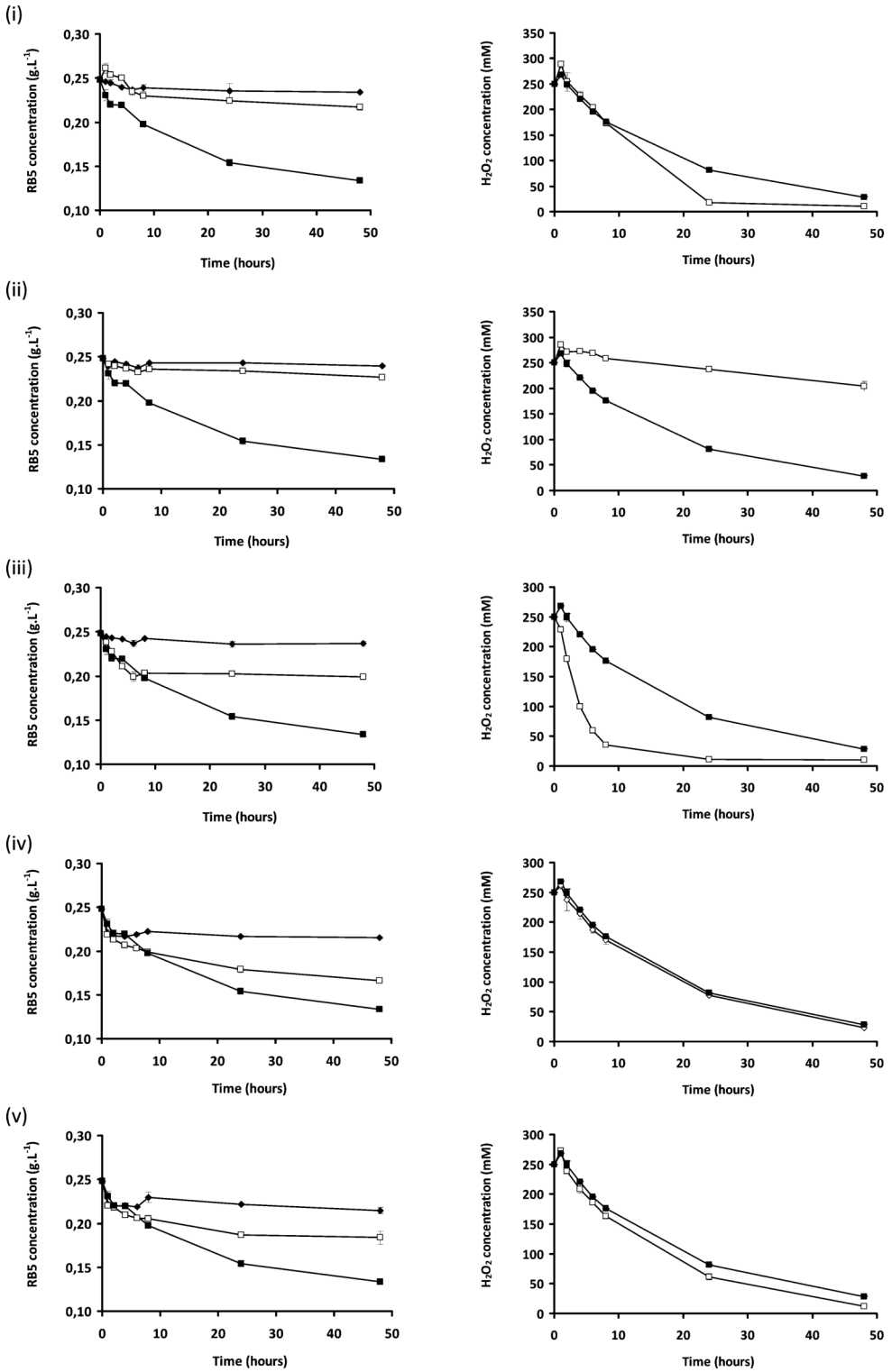

Fig. 6 Concentration of RB5 (left) and H_2O_2 (right) as a function of time in the presence of goethite + H_2O_2 (■), inorganic material + H_2O_2 (◆), goethite + H_2O_2 + inorganic material (□). Experiments were performed in 5 mL phosphate buffer with 20 mg goethite, 250 mM H_2O_2 and 10 mg inorganic material. The inorganic materials are listed as follows (i) aluminium titanate; (ii) antimony oxide; (iii) cerium oxide; (iv) titanium silicalite-1; (v) titanium xonotlite.

produce volatile antimony halogen compounds, which remove the high energy radicals that feed the flame phase of the fire, thus reinforcing the flame suppressing effect of the halogenated flame retardants.[31]Aluminium titanate and antimony oxide are able to protect RB5 from oxidative degradation. After 48 h, the RB5 concentration was at *ca.* 220 mg L^{-1} and *ca.* 230

mg L^{-1}, respectively – both significantly higher than the RB5 concentration of *ca.* 130 mg L^{-1} obtained when no protection with an inorganic anti-oxidant is provided. We monitored the H_2O_2 concentration as a function of time in the absence of RB5 to avoid interference. The consumption of H_2O_2 was found to be independent of the presence or absence of aluminium titanate. This observation strongly suggests that aluminium titanate is able to scavenge radicals, produced from H_2O_2 (or at least to enhance their termination/destruction). In this way, the RB5 molecules are protected from degradation.

Antimony oxide seems to work in a different way. The consumption of H_2O_2 was very low in the presence of antimony oxide. Whilst the exact mechanism responsible for the inhibition of H_2O_2 degradation by means of antimony oxide is beyond the scope this screening, it can be speculated that the prevention of RB5 degradation results from hindered H_2O_2 decomposition.

The investigated cerium oxide has particle sizes below 25 nm and a BET surface area of 54 m^2 g^{-1}. The anti-oxidant properties of cerium oxide have been documented in prior work.[19] It was somewhat unexpected to see that the RB5 concentration decreased slightly faster upon addition of cerium oxide during the first 6 h only (Fig. 5). After this initial drop, the RB5 concentration stabilized and remained relatively constant at *ca.* 200 mg L^{-1}. This is substantially higher than the final RB5 concentration of *ca.* 130 mg L^{-1} in the case of the standard degradation. Mechanistically, cerium oxide has been suggested to be a superoxide dismutase mimic due to the redox switch between Ce^{3+} and Ce^{4+}.[18] The present testing protocol, however, probes for the scavenging of radicals created by means of the Fenton reaction. A closer examination of the H_2O_2 consumption during the reaction when cerium oxide is added revealed that the H_2O_2 concentration decreased very quickly, and was completed within the first 6 h (Fig. 6). Cerium oxide caused decomposition of H_2O_2 into H_2O and O_2 *via* the facial one-electron switch of Ce^{3+}/Ce^{4+}. This side-reaction caused a fast decrease of the H_2O_2 concentration and, consequently, eliminated the reagent for the Fenton reaction. The point at which the H_2O_2 concentration approached zero corresponded well with the time at which the RB5 concentration was stabilized. This suggests that cerium oxide acts as a H_2O_2 decomposer in this screening protocol. However, it cannot be excluded that cerium oxide decomposes H_2O_2 to singlet oxygen which causes bleaching of the dye.

Titanium silicalite-1 (TS-1) and titanium xonotlite also showed a significant anti-oxidant capacity. They have no influence on the H_2O_2 consumption when added to the RB5 degradation reaction (Fig. 6). Titanium silicalite-1 tends to adsorb or degrade a small fraction of the RB5 molecules during the first 4 h of the experiment. At longer reaction times, it seemed that the addition of titanium silicalite-1 had a protective effect on the RB5 molecules. Indeed, after 48 h the RB5 concentration was *ca.* 20 mg L^{-1} upon the addition of titanium silicalite-1. The results obtained with titanium xonotlite are very similar to the case of titanium silicalite-1. Titanium xonotlite also tends to adsorb or degrade a small fraction of the RB5 molecules during the first 4 h of the experiment. After 48 h, the RB5 concentration had reached *ca.* 185 mg L^{-1}, which exceeds the 130 mg L^{-1} when no titanium xonotlite is added to the reaction vessel. Titanium silicalite-1 consists of small crystalline particles with sizes around 300 nm. Titanium xonotlite is comprised of fiber-like particles which are aggregated into larger structures of *ca.* 15 μm (Fig. 1). Both materials are microporous and their pore volumes are 0.2 mL g^{-1} and 0.07 mL g^{-1}, respectively. Titanium silicalite-1 (TS-1) is a zeolitic-type material with a MFI structure, showing high catalytic activity, efficiency and selectivity in oxidation reactions based on the use of H_2O_2 as oxidation agent, in mild reaction conditions such as aromatic hydroxylation, epoxidation of alkenes, ammoximation of cyclohexanone and oxidation of alkenes and alcohols.[32] Xonotlite is a calcium silicate and is known for its excellent insulating properties. It has an extremely low thermal conductivity.[33] Titanium xonotlite presents a xonotlite material in which a certain fraction of the Si atoms are replaced by Ti atoms.[32–34]

3.4 Spin-trapping and semi-quantitative EPR

The inorganic materials identified as potential anti-oxidants (Table 2) were later evaluated by spin-trapping and semi-quantitative EPR. This technique allowed us to directly measure the materials' capacity to scavenge radicals that were generated by the heterogeneous Fenton system. We added the spin-trapping agent DMPO to the reaction tube after 30 min and 4 h. The signal of the stable spin-adduct was measured with EPR after 15 min incubation, with double integration of this signal allowing for a semi-quantitative evaluation of the total spin concentration present in a particular sample. Fig. 7 shows that aluminium titanate and antimony oxide are able to reduce the radical concentration by 75% when compared to the value obtained under reference conditions with goethite and H_2O_2. Cerium oxide, titanium silicalite-1 and titanium xonotlite reduce this reference value down to 50%. The same trend is observed when the reaction is allowed to proceed for 4 h. Spin-trapping with DMPO and semi-quantitative EPR measurements hence confirm the results obtained in the screening protocol based on the heterogeneous Fenton

Table 2 Properties of the inorganic materials identified as potential anti-oxidants

Material	Specific surface area (m^2 g^{-1})	Pore volume (mL g^{-1})	Particle size
Aluminium titanate	193	/	<100 nm
Antimony oxide	83	/	<100 nm
Cerium oxide	54	/	<25 nm
Titanium silicalite-1	381	0.2	300 nm
Titanium xonolite	157	0.07	15 μm

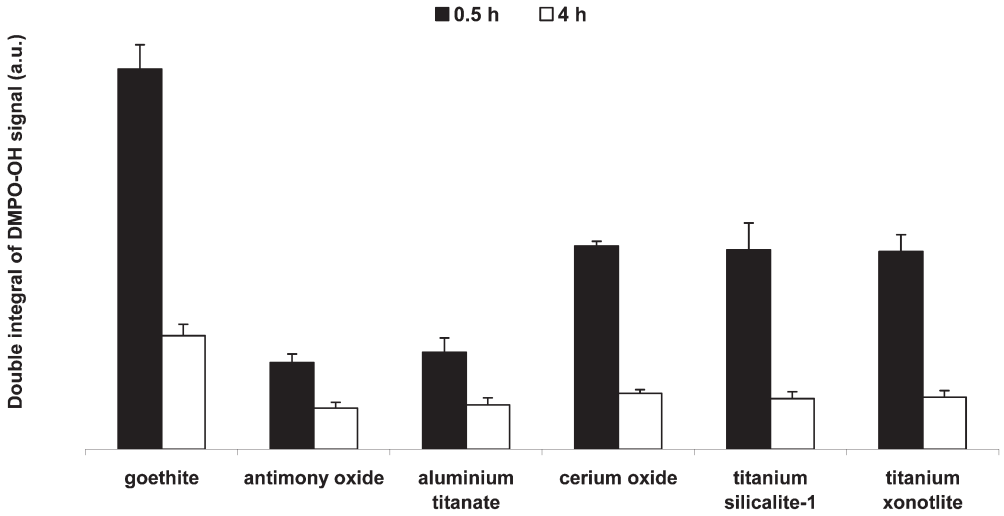

Fig. 7 Double integral values of the DMPO–OH signal. DMPO was added to the reaction vessel after 0.5 h (■) and 4 h (□). After 15 min incubation, the DMPO–OH signal was measured with EPR. Goethite represents the standard reaction with goethite and H_2O_2. The effect of the addition of antimony oxide, aluminium titanate, cerium oxide, titanium silicalite-1 and titanium xonotlite is presented.

degradation of dyes (Fig. 6). We emphasize that the screening protocol is far more efficient than the time consuming spin-trapping experiments to screen a large library of materials.

4 Conclusions

A convenient screening protocol was developed to evaluate the anti-oxidant and pro-oxidant capacity of inorganic oxides. The method is based on the heterogeneous Fenton degradation of a dye by the solid-state catalyst goethite in a phosphate buffer. With this rapid and simple protocol, we subsequently screened a material-library containing chemically and structurally different inorganic oxides. Not only did these tests confirm the known anti-oxidant capacity of cerium oxide, but they also identified four new materials with an anti-oxidant capacity: aluminium titanate, antimony oxide, titanium silicalite-1 and titanium xonotlite. In particular, the materials with titanium – either in a bulk phase or dispersed in mixed oxides with a different structure – show an excellent anti-oxidant capacity and deserve further attention.

The results obtained from the new protocol were confirmed by semi-quantitative EPR measurements. It appears that there may be alternative ways for a material to show an anti-oxidant capacity. The blocking or acceleration of H_2O_2 decomposition, and the scavenging of radicals were observed. Future work will be directed towards the elucidation of the physical chemistry underlying this scavenging behaviour.

Acknowledgements

RM acknowledges the Flemish FWO for a post-doctoral fellowship and a travelling grant. JM acknowledges the Flemish government for long term structural funding (Methusalem). IH is indebted to the ETH Zurich for financial support.

References

1 R. J. Mailloux and M. E. Harper, Uncoupling proteins and the control of mitochondrial reactive oxygen species production, *Free Radical Biol. Med.*, 2011, **51**, 1106–1115.
2 M. A. Puertollano, E. Puertollano, G. A. de Cienfuegos and M. A. de Pablo, Dietary Anti-oxidants: Immunity and Host Defense, *Curr. Top. Med. Chem.*, 2011, **11**, 1752–1766.
3 O. Ioannidis, I. Varnalidis, G. Paraskevas and D. Botsios, Nutritional Modulation of the Inflammatory Bowel Response, *Digestion*, 2011, **84**, 89–101.
4 J. M. Anderson, Biological responses to materials, *Annu. Rev. Mater. Res.*, 2001, **31**, 81–110.
5 W. E. Liu, M. L. Ma, K. M. Bratlie, T. T. Dang, R. Langer and D. G. Anderson, Real-time in vivo detection of biomaterial-induced reactive oxygen species, *Biomaterials*, 2011, **32**, 1796–1801.
6 J. Larsson, C. Persson, P. Tengvall and H. Lundqvist-Gustafsson, Anti-inflammatory effects of titanium-peroxy gel: Role of oxygen metabolites and apoptosis, *J. Biomed. Mater. Res.*, 2004, **68**, 448–457.
7 P. Thomsen and L. A. Ericson, Inflammatory cell response to bone implant surfaces, in *The Bone–Biomaterial Interface*, ed. J. E. Davies, Toronto Press, 1991, pp. 153–164.
8 D. M. Brunette, P. Tengvall, M. Textor and P. Thomson, Titanium in Medicine: Material science, Surface science, Engineering, Biological responses, *Medical applications*, Springer, 2001.
9 H. Sahlin, R. Contreras, D. F. Gaskill, L. M. Bjursten and J. A. Frangos, Anti-inflammatory properties of micropatterned titanium coatings, *J. Biomed. Mater. Res. A.*, 2006, **77**, 43–49.

10 S. Spriano, S. Ferraris, C. L. Bianchi, C. Cassinelli, P. Torricelli, M. Fini, L. Rimondini and R. Giardino, Titanium alloys: preparation, properties and applications, *Mat. Sci. Tech.*, 2010, 269–293.
11 R. Suzuki, G. Hirata, J. McKittrick and J. A. Frangos, Surface interaction of inflammatory species with titanium and titanium oxide, *MRS Online Proc. Libr.*, 1998, **530**, 111–116.
12 R. Contreras, H. Sahlin and J. A. Frangos, Titanate biomaterials with enhanced antiinflammatory properties, *J. Biomed. Mater. Res. A.*, 2007, **80**, 480–485.
13 J. J. Muyco, J. J. Gray, T. V. Ratto, C. A. Orme, J. McKittrick and J. A. Frangos, In situ characterization of Ti-peroxy gel during formation on titanium surfaces in hydrogen peroxide containing solutions, *Mater. Sci. Eng., C*, 2006, **26**, 1408–1411.
14 P. Tengvall, I. Lundström and E. H. Sjöqvist, Titanium-hydrogen peroxide interaction: model studies of the influence of the inflammatory response on titanium implants, *Biomaterials*, 1989, **10**, 166–175.
15 R. Suzuki and J. A. Frangos, Inhibition of Inflammatory Species by Titanium Surfaces, *Clin. Orthop. Relat. Res.*, 2000, **372**, 280–289.
16 C. M. Stanford, Surface Modification of Biomedical and Dental Implants and the Processes of Inflammation, Wound Healing and Bone Formation, *Int. J. Mol. Sci.*, 2010, **11**, 354–369.
17 D. Schubert, R. Dargusch, J. Raitano and S. W. Chan, Cerium and yttrium oxide nanoparticles are neuroprotective, *Biochem. Biophys. Res. Commun.*, 2006, **342**, 86–91.
18 E. G. Heckert, A. S. Karakoti, S. Seal and W. T. Self, The role of cerium redox state in the SOD mimetic activity of nanoceria, *Biomaterials*, 2008, **29**, 2705–2709.
19 A. Karakoti, S. Singh, J. M. Dowding, S. Seal and W. T. Self, Redox-active radical scavenging nanomaterials, *Chem. Soc. Rev.*, 2010, **39**, 4422–4432.
20 D. L. Vanoppen, D.E. De Vos and P. A. Jacobs, Ion-exchanged Y zeolites as catalysts for the liquid phase autoxidation of cyclohexane, *J. Catal.*, 1998, **177**, 22–28.
21 D. L. Vanoppen, D. E. De Vos, M. J. Genet, P. G. Rouxhet and P. A. Jacobs, Cobalt-containing molecular sieves as catalysts for the low conversion autoxidation of pure cyclohexane, *Angew. Chem., Int. Ed. Engl.*, 1995, **34**, 560–564.
22 C. Sanchez-Moreno, Review: Methods Used to Evaluate the Free Radical Scavenging Activity in Foods and Biological Systems, *Food Sci. Tech. Int.*, 2002, **8**, 121–137.
23 M. Hartmann, S. Kullmanna and H. Kellerb, Wastewater treatment with heterogeneous Fenton-type catalysts based on porous materials, *J. Mater. Chem.*, 2010, **20**, 9002–9017.
24 G. Mathys, G. Tosin, J. Franken, J. Martens and M. Janssen, *Olefin oligomerization process. European patent application*, Patent number 11187214.9-1211.
25 J. A. Martens, P. Buskens, P. A. Jacobs, A. Vanderpol, J. H. C. Vanhooff, C. Ferrini, H. W. Kouwenhoven, P. J. Kooyman and H. Vanbekkum, Hydroxylation of phenol with hydrogen-peroxide on eurots-1 catalyst, *Appl. Catal., A*, 1993, **99**, 71–84.
26 J. A. Martens, P. J. Grobet and P. A. Jacobs, Catalytic Activity and Si, Al, P ordering in Microporous Silicoaluminophosphates of the SAPO-5, SAPO-11 and SAPO-37 Type, *J. Catal.*, 1990, **126**, 299–305.
27 J. A. Martens and P. A. Jacobs, in *Catalysis and Zeolites, fundamentals and applications*, ed. J. Weitkamp *et al.*, Springer, 1999, ch. 2, pp. 53–80.
28 R. Mellaerts, C. A. Aerts, J. Van Humbeeck, P. Augustijns, G. Van den Mooter and J. A. Martens, Enhanced release of itraconazole from ordered mesoporous SBA-15 silica materials, *Chem. Commun.*, 2007, **13**, 1375–1377.
29 W. H. Koppenol, The Haber–Weiss cycle – 70 years later, *Redox Rep.*, 2001, **6**, 229–234.
30 J. I. Hubert, A. K. Vasudevan, G. Aruldhas, A. D. Damodaran and K. G. K. Warrier, FTIR as a Tool to Study High-Temperature Phase Formation in Sol–Gel Aluminium Titanate, *J. Solid State Chem.*, 1997, **131**, 181–184.
31 S. Zhang and A. R. Horrocks, A review of flame retardant polypropylene fibres, *Prog. Polym. Sci.*, 2003, **28**, 1517–1538.
32 A. Vasile and A. M. Busuioc-Tomoiaga, A new route for the synthesis of titanium silicalite-1, *Mater. Res. Bull.*, 2012, **47**, 35–41.
33 G. S. Wei, X. X. Zhang and F. Yu Thermal, Conductivity measurements on xonotlite-type calcium silicate by the transient hot-strip method, *J. Uni. Sci. Tech. Beijing*, 2008, **15**, 791–795.
34 O. Anton and D. Van Wouwe, *Synthetic crystal aggregates of xonotlite and process for preparing same*, Patent number 86116215.4.